Second-order Born-Rytov prestack depth imaging demonstrated on a field data set

Alexander Druzhinin, Edinburgh Anisotropy Project, British Geological Survey, Jan Pajchel†, Steen Petersen†, †Norsk Hydro, and Philippe Thierry, École des Mines de Paris*

Summary

We develop an efficient method to solve a nonlinear inverse acoustic scattering problem based upon the second-order Born-Rytov approximation. The key point is a dipole-scatterer response which accounts for the waves interacting repeatedly with the scatterers. A numerical algorithm is demonstrated on a field data set (Oseberg Field, North Sea). The results show that this accurate and efficient imaging method avoids severe restrictions on the choice of initial velocity model and yields a better quality of image than the traditional linearized approach. It is capable of retrieving a new structural and velocity information in a strongly scattering medium that is known with only a limited accuracy.

Introduction

Existing prestack depth imaging techniques are mainly of the linearized type, i.e. they are based upon the first-order Born or Rytov approximation of weak scattering (Wu and Toksöz, 1987; Burridge et al., 1998). In a strongly scattering medium, nonlinear terms of the Neumann series related to multiply-scattered waves are often not negligible (Weglein et al., 1997; Scales and Snieder, 1997). It is then challenging to make use of them to achieve a higher resolution of the image (Reiter et al., 1991). The overall aim is to derive global statistical properties of the reservoir with reduced uncertainties.

In this paper, we obtain an explicit noniterative solution to nonlinear inverse scattering problems beyond the validity of the first-order Born-theory, based upon the second-order Born-Rytov approximation (Yura et al., 1983; Weglein et al., 1997), which accounts for the waves interacting twice with the target points. Our purpose is to eliminate the well-known sensitivity of the Born model to the input background velocity. Questions of optimal numerical implementation are addressed and applications to field data are presented.

Second-order Born-Rytov depth imaging

Let Σ be the acquisition surface in which the source-receiver pairs $\mathbf{r}_{s,g}$ are defined. This set of observations constitutes the reduced harmonic wavefield

$$D(\mathbf{r}_{s,g}) = \begin{cases} u(\mathbf{r}_{s,g}) - u_0(\mathbf{r}_{s,g}) & Born \\ \ln\left[u(\mathbf{r}_{s,g})/u_0(\mathbf{r}_{s,g})\right] u_0(\mathbf{r}_{s,g}) & Rytov \end{cases} \tag{1}$$

to be migrated to the scattering volume V. We calculate the background wavefield $u_0(\mathbf{r}_{s,g})$ and study the second-order scattering effect associated with a coupled secondary source at $\mathbf{r}_{1,2} \in V$ being referred to as the *dipole*. We define the dipole object function as a product $O(\mathbf{r}_1, \mathbf{r}_2) = O(\mathbf{r}_1)O(\mathbf{r}_2)$ expressed in terms of the point-source object functions $O(\mathbf{r}_{1,2})$ by Wu and Toksöz (1987). The second-order Born-Rytov approximation mentioned above represents a two-fold scattering integral over the volume V (Yura et al., 1983; Weglein et al., 1997). This integral is an explicit relationship between the wavefield (1) and the dipole object function $O(\mathbf{r}_1, \mathbf{r}_2)$. Its Generalized Radon Transform (GRT) (Burridge et al., 1998) gives the following new multi-shot backscattering formula

$$O(\mathbf{r}_1, \mathbf{r}_2) = (2\pi)^{-4} \int_\Sigma \int_\Sigma \frac{D(\mathbf{r}_{s,g})}{G} J_s J_g \partial^2 \mathbf{r}_{s,g}, \tag{2}$$

where $J_{s,g}$ is the well-known GRT acquisition Jacobian and G is the product of the free-space Green's functions $g(\mathbf{r}_s, \mathbf{r}_2)$, $g(\mathbf{r}_1, \mathbf{r}_2)$, and $g(\mathbf{r}_1, \mathbf{r}_g)$ in the background medium. Equation (1) can be used to estimate the squared velocity perturbation

$$\Delta c^2(\mathbf{r}_1)/c_0^2(\mathbf{r}_1) \simeq \sqrt{O(\mathbf{r}_1, \mathbf{r}_2)} \pm \varepsilon \tag{3}$$

together with the error bounds

$$\varepsilon^2 \simeq |O(\mathbf{r}_1, \mathbf{r}_2) - O(\mathbf{r}_2, \mathbf{r}_1)|$$

Theoretically, the object function must be symmetrical thanks to reciprocity. However, $\varepsilon \neq 0$ because eq. (1) contains different types of noise as well as unremoved higher-order scattering effects. Also, we recall that our acoustic formulation ignores shear and converted waves.

Our final goal is to recover the velocity perturbation from eq. (3) by dividing the target V into a set of cells. Traditionally, each cell is represented by a set of independent pixels, and it is assumed that pixels are

independent of their neighbors. The present scheme relaxes these assumptions due to the dipole sampling of the target.

Equation (2) represents an infinite integral over the observation array. Since this array is both discrete and finite in extent, we must deal with the restrictions in the numerical implementation of eq. (2). The spatial Nyquist criterion is one aspect that many integral methods have in common (Abma et al., 1999). To prevent migration aliasing effects, the traces are convolved with the spike-like filter $\left(t^2-\tau^2\right)^{-1/2}$, where $\tau = \tau(\mathbf{r}_s, \mathbf{r}_2, \mathbf{r}_1, \mathbf{r}_g)$ is the total traveltime "source-dipole-receiver". Traditional operator truncation (Abma et al., 1999) is also implemented. Aperture truncation artifacts are removed by using model-based arrival angle information (Takahashi, 1995).

The Oseberg field example

The method was tested on a marine data set NH8906 acquired by Norsk Hydro from the Oseberg Field, in the Norwegian sector of the North Sea. For the sake of simplicity, only one line (number 16) was analysed. It consists of 500 shots with 120 traces per shot. Both the shot and the receiver spacing were 25 m. The initial velocity model by Tura et al. (1997) was transformed into the squared slowness. It was highly oversampled in the crossline direction using the B-splines for more accurate ray tracing done by Thierry et al. (1996). Ray tracing was performed in a gentle macro-velocity model with weak lateral velocity variations. We compute the amplitudes, traveltimes, and slowness vectors appearing in eq. (2) over a regularly sampled target for each source-receiver position. This takes almost the same CPU time as traditional true-amplitude depth imaging (Thierry et al., 1996; Tura et al., 1997). We selected a 15 km$\times$ 0.6 km target zone located at a depth 2.4 km containing a reservoir. The target covers sections of the Gamma and Alpha fault blocks shown by Tura et al. (1997). The bin size was 25 m$\times$ 5 m.

Figures 1 to 3 compare results obtained using eq. (2) (Rytov) with the first-order Rytov inverse (Wu and Toksöz, 1987) in space-time variables. The Common Image Point gathers are compared in Figure 1. An improvement in vertical resolution is apparent at near offsets (see bottom panel in Fig.1). As a result, the bottom image in Fig.2 is better defined in terms of resolution than the top image in Fig.2, except for the rather cosmetic effect of image aliasing. Finally, Figure 3 shows the results of imaging after cell discretization of the target for reservoir simulation purposes. In this example, the first-order imaging (top panel) yields almost constant velocity in the most interesting part of the reservoir ($x \leq 6$ km), whereas eq. (2) predicts sufficiently well the lateral velocity variations. These variations are consistent with images in Fig.2 and a priori geological information.

Conclusions

We have developed a high-resolution prestack depth imaging technique based upon the second-order Born-Rytov approximation. The explicit inversion operator accounts for the waves interacting twice with the dipole-type elementary scatterers. A fast anti-aliased numerical version of this operator has been implemented using the same methodology as that used in the GRT methods. Unlike existing nonlinear iterative inversion schemes, the final algorithm is not time-consuming and does not require fairly accurate a priori knowledge of the velocity model.

The method has been applied to a marine data set from the Oseberg Field, North Sea. The results show that the resolution ability of the new method is much higher than those of traditional first-order Born-Rytov inversion techniques. After a sparse sampling of the target for fluid-flow monitoring, it is still capable of characterizing the reservoir.

Acknowledgments

This work was supported by the Commission of the European Communities, Grant No. JOF3CT970029. We are grateful to Norsk Hydro for providing the field data set. We express sincere thanks to Paul Henni (BGS) for helpful comments.

References

Abma, R., Sun, J., and Bernitsas, N., 1999, Antialiasing methods in Kirchhoff migration: Geophysics, **64**, 1783-1792.

Burridge, R., de Hoop, M., Miller, D., and Spencer, C., 1998, Multi-parameter inversion in anisotropic media: Geophys. I. Internat., **134**, 757-777.

Reiter, E.C., Toksöz, M.N., Keho, T.H., and Purdy, G.M., 1991, Imaging with deep-water multiples: Geophysics, **56**, 1081-1086.

Scales, J.A., and Snieder, R., 1997, Humility and nonlinearity: Geophysics, **62**, 1355-1358.

Takahashi, T., 1995, Prestack migration using arrival angle information: Geophysics, **60**, 154-163.

Thierry, P., Lambare, G., Podvin, P., and Noble, M., 1996, 3D prestack preserved amplitude migration: application to real data: 66th Ann. Internat. Mtg., Soc. Expl. Geophys., Expanded Abstracts, 555-558.

Tura, A., Hanitzsch, C., and Calandra, H., 1997, 3-D AVO migration/inversion of field data: Journal of Seismic Exploration, **6**, 117-125.

Weglein, A.B., Gasparotto, F.A., Carvalho, P.M., and Stolt, R.H., 1997, An inverse-scattering series method for attenuating multiples in seismic reflection data: Geophysics,**62**, 1975-1989.

Wu, R-S., and Toksöz, M.N., 1987, Diffraction tomography and multisource holography applied to seismic imaging: Geophysics, **52**, 11-25.

Yura, H.T., Sung, C.C., Clifford, S.F., and Hill, R.J., 1983, Second-order Rytov approximation: J. Opt. Soc. Am. A, **73**, 500-502.

Figure 1: Common-Image Gathers

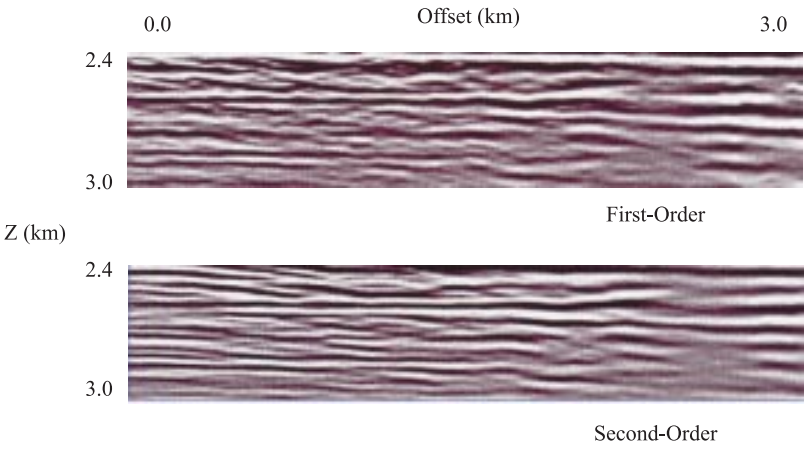

Figure 2: Depth Migrated Sections

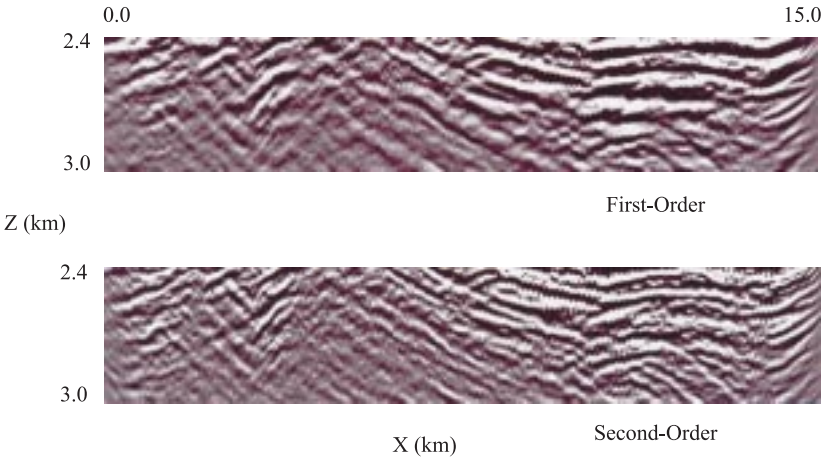

Figure 3: Handling Sparse Grid for Fluid-Flow Monitoring